carine crystallography 3.1 manual

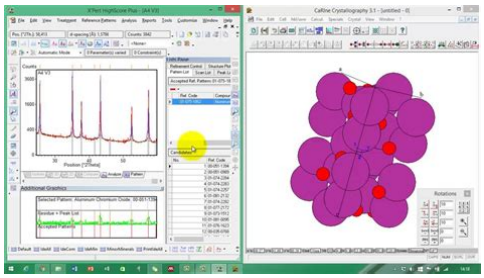

File Name: carine crystallography 3.1 manual.pdf
Size: 4022 KB
Type: PDF, ePub, eBook
Category: Book
Uploaded: 11 May 2019, 21:15 PM
Rating: 4.6/5 from 657 votes.

Status: AVAILABLE

Last checked: 9 Minutes ago!

In order to read or download carine crystallography 3.1 manual ebook, you need to create a FREE account.

Download Now!

eBook includes PDF, ePub and Kindle version

Book Descriptions:

We have made it easy for you to find a PDF Ebooks without any digging. And by having access to our ebooks online or by storing it on your computer, you have convenient answers with carine crystallography 3.1 manual . To get started finding carine crystallography 3.1 manual , you are right to find our website which has a comprehensive collection of manuals listed.
Our library is the biggest of these that have literally hundreds of thousands of different products represented.

Book Descriptions:

carine crystallography 3.1 manual

To browse Academia.edu and the wider internet faster and more securely, please take a few seconds to upgrade your browser. You can download the paper by clicking the button above. Related Papers CURSO By jhonatan cruz martinez APUNTES DE DISENO ASISTIDO POR COMPUTADORA By Giancarlo Z APUNTES DE DISENO ASISTIDO POR COMPUTADORA PARA INGENIERIA CIVIL By Andres lopez Curso AutoCAD By Karla Hernandez Perez CURSO DE AUTOCAD By Isaac Jalil READ PAPER Download pdf. Download it to learn how it became easy to create complex structures. Get the last version of CaRIne. CaRIne brings them together in a friendly graphic user interface. This is time and cost saving. The CaRIne software is organised around modular and upgradable projects which allow the addition of new modules for the next versions to come without modifying at all the software organisation. A new program for full operation of stereographic projections and indepth exploration of crystallographic orientation relationships is described. It is specifically designed for materials researchers who are in need of tools for extensive crystallographic analysis. The difference from other popular commercial software for crystallography is that this program provides new options for users to plot and fully control stereographic projections of an arbitrary pole centre for an arbitrary crystal structure and to illustrate composite stereographic projections, which are necessary to explore the orientation relationships between two phases. The program is able to perform a range of essential crystallographic calculations. Keywords stereographic projection; orientation relationships; computer programs. Read article Similar articles Supporting information Zip compressed file SP2 and reference manuals Chinese and English. This function isespecially useful in case of a network utilization.http://www.ronjenner.nl/userfiles/bosch-maxx-manual-download.xml

- **carine crystallography 3.1 manual, carine crystallography 3.1 manual, carine crystallography 3.1 manual pdf, carine crystallography 3.1 manual download, carine crystallography 3.1 manuals, carine crystallography 3.1 manual free.**

Inwhich case the choice of system from the Cell Menu is followed by the choiceof mode from the corresponding submenu primitive, bodycentred, basecentred, facecentred.CaRIne then opens a dialoguebox which allows the modification of the cellparameters respecting the system and a sphere is assigned to each point of thelattice. Obviously this sphere can be considered as an atom, and assigned achemical symbol using Mendeleev s Periodic Table, which is available.However, this is not required, the spheres can also be assimilated to simplelattice points.CaRIne and the crystallography 13At this point, it would be preferable to be able to substitute a motif at eachlattice point, and this function will be developed in a future version of CaRInein which the lattice points and the atoms will be clearly distinguished. At themoment, this substitution can be made by using space groups. The choice of agroup leads to a dialoguebox where the position of nonequivalent sites areentered. This defines a motif which will be repeated according to the group selements of symmetry. The space group characterises thesymmetry of a crystalline structure in the same way that a point groupcharacterises the symmetry of the exterior form of the crystal and the symmetryof its macroscopic properties. There are 32 point groups of symmetry 32crystalline classes.Each point group corresponds to several space groups. From the space group,the point group is obtained by eliminating all the translations. On the otherhand, space groups can be deduced from the point groups. In order to do this,an examination of all the possible combinations between the symmetryelements of the point group and the translations of the type of lattice allowed bythe point group is necessary.230 space groups can be obtained. Thisis possible with CaRIne. Angstroms A

XRD and interplanar distances listinterplanar distance dhkl Angstroms Asum of squared indices ind2 without unit interplanar distances listBragg angle.http://www.magneticmicrosphere.com/userfiles/bosch-maxx-user-manual.xml

Angstroms A identification of planescamera length L centimetres cm identification of planescamera constant K cm.A identification of planesdistances on diffraction patterns r1and r2centimetres cm.A identification of planeszone axis without unit cf.Thefunction associated with “real lattice“ windows are described throughout thischapter. At the bottom of such a window, a status bar which gives the angleof view, the current command and the cell parameters, can be found.The status barThe status bar is composed of 4 sections. In order to change the sections,click on the status bar. Each section is composed of angles which define theangle of view and the command associated with the lattice at the time.A command can be selected from a menu, using the mouse, thecorresponding short key or by using the tool palettes. When the download procedure has been completed, doubleclick the downloaded file to run WinZip and extract the archive into a directory of your choice. Note for Windows XP, extract all the content of the dowloaded archive to install the package extractor. 2 This trial version includes many tutorials to show how it is easy to create complex structures with version 4. This trial software is intended for evaluation purposes only. 3 The trial version of CaRIne 4.0 for Linux will be available soon. If you wish to be informed about the availability of this trial version please send an email to Cyrille Boudias. If you wish to be informed about the availability of this trial version please send an email to Cyrille Boudias. Previous article in issue Next article in issue Keywords antimony copper lithium oxide. All rights reserved. Recommended articles No articles found. Citing articles Article Metrics View article metrics About ScienceDirect Remote access Shopping cart Advertise Contact and support Terms and conditions Privacy policy We use cookies to help provide and enhance our service and tailor content and ads. By continuing you agree to the use of cookies.

When the download procedure has been completed, doubleclick the downloaded file to run WinZip and extract the archive into a directory of your choice. Note for Windows XP, extract all the content of the dowloaded archive to install the package extractor. 2 This trial version includes many tutorials to show how it is easy to create complex structures with version 4. This trial software is intended for evaluation purposes only. 3 The trial version of CaRIne 4.0 for Linux will be available soon. If you whish to be informed about the availability of this trial version please send an email to.Download the CaRIne trial packages corresponding to your operating systemIf a package extractor has already been installed on your computer. Bleach Vs Naruto 3.1 download the package corresponding to your operating system. Copy it in the pkg directory of the package extractor. In the latter case, pleaseUnder this harsh environment, the main factor limiting the service life of zirconium cladding, and hence fuel burnup efficiency, is water corrosion. This oxidation process has recently been linked to the presence of a suboxide phase with welldefined composition but unknown structure at the metaloxide interface. In this paper, the combination of firstprinciples materials modeling and highresolution electron microscopy is used to identify the structure of this suboxide phase, bringing us a step closer to developing strategies to mitigate aqueous oxidation in Zr alloys and prolong the operational lifetime of commercial fuel cladding alloys. This may be because the snippet appears in a figure legend, contains special characters or spans different sections of the article. The copyright line for this article was changed on December 3, 2014 after original onlineReceived 2014 Mar 17; Accepted 2014 May 29. Co. KGaA, Weinheim This is an open access article under the terms of the Creative Commons Attribution License, whichAssociated Data Supplementary Materials Fig. S1.

Image showing the region the diffraction pattern was obtained from a, theEnvironmental applications of organoclays for sorption of phenolEELS spectra c from the three different regions marked in theThe data fromOxygen Kedge EELS spectra c from the three different regions markedUnder this harsh environment, the main factor limiting the service lifeThis oxidation

processIn this paper, the combination ofMuch effort has gone into optimizing these materialsWhen the oxide isMany authors have described aA cubic ZrO phase has been reported at thisInterestingly, this layerEven though we cannot be sure if the ZrOThere is no known stable bulk form of ZrO.Very recently. Prediction of new, unknown, crystal structures has long been a challenge for theoreticians. InThere has been particular success identifying highpressureTo identify the structure of the suboxide material, we propose to first obtain the lowest energyThe growth ofIf a low energyIn this case, the experimental data availableZr x O Y stoichiometries. The search identifiedZrO 2 and Zr 3 O. The first structure is orthorhombic Figure 1 a, the second is hexagonal FigureDespite being structurally rather different, the orthorhombic andThus, we consider both the orthorhombic andWe now evaluate theWe note that isolatingThe fit between the other three experimentalIn cases where a particular experimental pattern could not be matched by aThe hexagonal structure isOpen in a separate window Fig 2 Fitting error of simulated diffraction data from each of the three different structures withWe also obtained a series of lowloss EELS spectra across the interface region. The spectra canZrO 2 spectrum on the other. In between there is a region in which the spectrum is not aExamples of these three spectra are given in Figure 3 and in the Supporting Information Figure S3 .

The peak positions for the different spectraWe focus on the first 30Higher level calculations have shown theThe comparison of experimental and computedHowever, this anisotropyWe note that small variations are seen in the experimental dataOpen in a separate window Fig 3 Experimental lowloss EELS spectra from the metal, suboxide, and oxide. Table 1 Peak positions for the experimental EELS spectra collected from the metal, suboxide, and oxideThis conclusion does not change if the orientation dependenceThe intensities of the peaks are also significant, but these are moreThe oxygen Kedge was also obtained experimentally across the interface region, although the lackSimulated spectra from the three candidate structures can be seen in the Supporting InformationThe zirconium. L 2,3 edge obtained from the interface region showed a systematic downwards shift inInformation Figure S10 . In summary, the hexagonal structure is the only candidate ZrO structure, which is both calculatedWe thereforeThe AIRSS algorithm produced two energetically equivalent structures, soThe suboxide grains form at theThe Zr metal also has a hexagonal structure, and the metal immediatelyWe suggest that the crystallographicImportantly, neitherThis work not only provides an answerRecrystallized samples were corrosion tested by EDF in a staticTo study the progression of the oxidation, samples spent varyingThis study focuses on two Zircaloy4 samples, which have spentAll of the zirconium alloy samples showed phases atSupporting Information was obtained from a ZIRLO sample, which had been oxidized for 100 days. 5.2. Electron Microscopy Convergent beam electron diffraction patterns were obtained from regions at the interface using a. Philips CM20 TEM operated at 200 kV. The convergent beam is used to limit the volume of the specimenEnfina spectrometer. The energy resolution was 0.6 eV measured at a dispersion of 0.2 eV per pixelThe spectra were collected in 0.

25 nm stepsSymmetry constraints were used, with spaceThree thousand thirtytwo structures were generated in total, with 1162 forCrystallography 3.1, which employs the structure factor method. The parameters used for the EELS calculationsA Gaussian broadening of 2.0 eVA supercell was used to separate the periodic imagesTechnical support issues arising from supporting information other thanEnvironmental applications of organoclays for sorption of phenolEELS spectra c from the three different regions marked in theThe data fromOxygen Kedge EELS spectra c from the three different regions markedIn Zirconium in the Nuclear Industry Twelfth International Symposium. Sabol GP, Moan GD, editors.How are we doing. Europe PMC is part of the ELIXIR infrastructureEurope PMC is a service of theIt includes content provided to the. I have read and accept the Wiley Online Library Terms and Conditions of Use Shareable Link Use the link below to share a fulltext version of this article with your friends and colleagues. Learn more. Copy URL Under this harsh environment, the main factor limiting the service life of zirconium cladding, and hence fuel burnup efficiency, is water

corrosion. In this paper, the combination of firstprinciples materials modeling and highresolution electron microscopy is used to identify the structure of this suboxide phase, bringing us a step closer to developing strategies to mitigate aqueous oxidation in Zr alloys and prolong the operational lifetime of commercial fuel cladding alloys. Much effort has gone into optimizing these materials to withstand the harsh service environments and to contribute to the safe operation and long lifetime of these reactors. 1 The main factor limiting the service life of zirconium cladding and hence fuel burnup efficiency is water corrosion. 1 Many authors have described a thin “intermediate” or “suboxide” layer at this interface, for instance phases with stoichiometry Zr 3 O 3 or 40 at% O 4 have been reported.

More recently, electron energy loss spectroscopy EELS 5 and atom probe tomography 6, 7 have identified a layer of composition very close to ZrO at the interface between the metal and the oxide under conditions of slow oxide growth before the first abrupt transition to faster oxidation kinetics. A cubic ZrO phase has been reported at this interface, 8, 9 but this identification has been challenged, 10, 11 and despite considerable experimental effort, the structure of the ZrO suboxide is still unknown. Interestingly, this layer is not found during the fast, posttransition stage of oxidation, and this is one of the most obvious microstructural changes as the rate increases.A cubic rocksalt structure 12 14 has previously been suggested to exist, however, it has not been possible to find an unambiguous experimental report of this structure in the literature see Supporting Information. Very recently, Puchala and Van der Ven 15 have used a cluster expansion approach to predict a stable hexagonal ZrO phase based on the TiO structure. Prediction of new, unknown, crystal structures has long been a challenge for theoreticians. In recent years, approaches using numerical techniques such as genetic algorithms, 16 20 particle swarm, 21 and random structure generation 22 have been shown to be capable of predicting new phases of materials. There has been particular success identifying highpressure phases of simple materials e.g., 23 , with several ab initio predictions subsequently being confirmed experimentally.The growth of the layer will be influenced by its interface to the metal and we therefore do not expect the suboxide layer observed experimentally to necessarily be the structure with the lowest formation energy, although it should be among the set of structures with the lowest energies.

In this case, the experimental data available for comparison includes electron diffraction, a direct probe of the atomic arrangement, and electronenergy loss experiments, which are a sensitive probe of the electronic structure of the material.The search identified two low energy ZrO structures, which are energetically stable with respect to decomposition into ZrO 2 and Zr 3 O. The first structure is orthorhombic Figure 1 a, the second is hexagonal Figure 1 b and isostructural with TaN. 25 This hexagonal structure is the same as that recently predicted by Puchala and Van der Ven 15 on the basis of its similarity to phases in the TiO system. Despite being structurally rather different, the orthorhombic and hexagonal structures have predicted formation energies within 0.002eV per formula unit of each other. Cubic ZrO was not found by the AIRSS algorithm, which is consistent with previous calculations, which reported it to be mechanically unstable as a bulk phase. 11 We find its formation energy to be 1eV per formula unit higher than the orthorhombic and hexagonal phases. Thus, we consider both the orthorhombic and hexagonal structures to be candidate structures for the ZrO phase and we also include the cubic structure for consideration due to its previous prominence in the literature. We now evaluate the candidate structures by comparing their predicted properties with experiment.Using a crystallography software package, 26 the fit with the experimental data was evaluated for each of the candidate structures by summing the relative errors in both interplanar distances and angles see Supporting Information. Two of the experimental patterns were not matched by any of the candidate structures. The fit between the other three experimental diffraction patterns and the proposed structures is summarized in Figure 2. In cases where a particular experimental pattern could not be matched by a candidate structure, an arbitrarily large error has been included.

The hexagonal structure is consistent with all three diffraction patterns, the cubic structure with two while the orthorhombic structure is not consistent with any of the experimental data.The spectra can be seen to change from that of Zr metal on one side of the interface to the characteristic ZrO 2 spectrum on the other. In between there is a region in which the spectrum is not a linear combination of the other two. Examples of these three spectra are given in Figure 3 and in the Supporting Information Figure S3. The peak positions for the different spectra are summarized in Table 1. EELS spectra have been simulated for each of the candidate structures using DFT and the random phase approximation excluding local field effects RPANLF Figure 4 . We focus on the first 30eV of the spectra as this is the most diagnostic region. Higher level calculations have shown the RPANLF approach to be reliable in this energy regime. 27 The positions of the peaks simulated from the three different structures are listed in Table 1, along with a simple estimate of their match to the experimental data from the suboxide region. The comparison of experimental and computed spectra is complicated by the fact that the spectra from the hexagonal and orthorhombic structures depend on the orientation of the crystal with respect to the electron beam. However, this anisotropy is very small for the orthorhombic case and mainly affects the peak intensities in the hexagonal case see Supporting Information. We note that small variations are seen in the experimental data recorded from the interface region both in different parts of a sample and in different samples Supporting Information Figure S4. This may indicate a small orientation dependence in the spectra as the data may correspond either to grains in different orientations or from multiple grains.This conclusion does not change if the orientation dependence is also taken into account see Supporting Information Table S1.

The intensities of the peaks are also significant, but these are more difficult to compare with experiment due to the presence of the zeroloss peak at 0eV in the experimental data. The three peaks at 14.6, 17.4, and 24.2eV are all of a similar height in the experimental data. These features are well matched by the data simulated from the hexagonal and orthorhombic structures, but less well matched the cubic structure where the spectrum shows a reduction in intensity for the second of the three peaks. Simulated spectra from the three candidate structures can be seen in the Supporting Information Figure S8 and both the hexagonal and orthorhombic structures are consistent with the experimental data. The zirconium L 2,3 edge obtained from the interface region showed a systematic downwards shift in energy from the oxide to the metal consistent with a decrease in oxidation number see Supporting Information Figure S10.We therefore propose that the suboxide phase has the hexagonal structure shown in Figure 1 b. The bandstructure and density of states of the structure are shown in the Supporting Information. The AIRSS algorithm produced two energetically equivalent structures, so why might the hexagonal phase be favored over the orthorhombic. The suboxide grains form at the boundary between the ZrO 2 and the Zr metal by transport of the oxidizing species through the oxide and into the metal. We suggest that the crystallographic similarity between the Zr metal and hexagonal ZrO structures may be the reason this phase forms in preference to the orthorhombic phase.This work not only provides an answer to an important technological question, but also showcases the power of this combination of techniques. To study the progression of the oxidation, samples spent varying amounts of time inside the autoclave. This study focuses on two Zircaloy4 samples, which have spent 34 and 90 days in the autoclave and two ZIRLO samples, which have spent 34 and 100 days in the autoclave.

6 The spectra were collected in 0.25nm steps and 50 0.04s exposures were combined for each pixel to give a total integration time of 2s. The AIRSS runs have been performed at 0GPa for unit cells containing up to six ZrO formula units, and a variety of other compositions. Symmetry constraints were used, with space groups chosen randomly. Three thousand thirtytwo structures were generated in total, with 1162 for the ZrO composition. Relatively coarse convergence parameters were employed during the searches, with a cutoff energy of 340eV, and a kpoint sampling of 2 0.1 A 1 or less.The parameters used for the EELS calculations were the same as for the geometry

optimizations, except that the kpoint sampling was increased until any further increases had no effect on the simulated spectrum. A Gaussian broadening of 2.0eV was applied to the simulated loss function for direct comparison with the experimental data. The core hole was included in the oxygen Kedge simulations by constructing an oxygen pseudopotential with an electron removed form the 1s orbital. A supercell was used to separate the periodic images of the core hole so that interactions between them did not affect the simulated spectra. The theoretical spectra were broadened using a Gaussian to represent the energy spread of the electron beam, a fixed Lorentzian to represent the broadening due to the finite lifetime of the initial state and an energy dependent Lorentzian to represent the broadening due to finite lifetime of the final state.Such materials are peer reviewed and may be reorganized for online delivery, but are not copyedited or typeset. Technical support issues arising from supporting information other than missing files should be addressed to the authors. Environmental applications of organoclays for sorption of phenol and its derivatives. EELS spectra c from the three different regions marked in the image and on the spectrum image.

Oxygen Kedge EELS spectra c from the three different regions marked in the image and on the spectrum image. Any queries other than missing content should be directed to the corresponding author for the article. The portal can access those files and use them to remember the users data, such as their chosen settings screen view, interface language, etc., or their login data. By using the Infona portal the user accepts automatic saving and using this information for portal operation purposes. More information on the subject can be found in the Privacy Policy and Terms of Service. By closing this window the user confirms that they have read the information on cookie usage, and they accept the privacy policy and the way cookies are used by the portal. You can change the cookie settings in your browser. It allow to create list of users contirbution. Assignment does not change access privileges to resource content. Are you sure SYNAT “Interdisciplinary System for Interactive Scientific and ScientificTechnical Information”. Follow our stepbystep guide. Please enable JavaScriptCenter of Excellence for Semiconductor Lighting and Display, Nanyang Technological University, Singapore 639798, SingaporeThe crystal qualities of both the resultant In 2 O 3 and the remaining InN were significantly improved by using CRTA instead of RTA. Microscopic and spectroscopic analyses, together with the effect of Si 3 N 4 encapsulations, provide evidence that the oxidation of InN is realized by oxygen inward diffusion. The oxygen inward diffusion is slowed down and the thermal decomposition of InN is suppressed by using CRTA, which in turn leads to a layerbylayer oxidation of InN. Try again XX with permission from the Centre National de la RechercheXX with permission from the PCCP Owner Societies.XX with permission from the European Society for Photobiology,XX with permission from The Royal Society of Chemistry.XX is the XXth reference in the list of references.This may take some time to load.

Follow our stepbystep guide. Please enable JavaScriptRamakrishnan, a Nair, a Dhakshinamoorthy, a Pullithadathil Try again XX with permission from the Centre National de la RechercheXX with permission from the PCCP Owner Societies.XX with permission from the European Society for Photobiology,XX with permission from The Royal Society of Chemistry.XX is the XXth reference in the list of references.This may take some time to load. Chapters dedicated to RNA preparation and crystallogenesis will be of interest to beginners, while chapters focused on data collection, phasing and refinement will be particularly useful to researchers with a higher level of expertise. Several functional case studies are also presented in the last part of the book. Written in the highly successful Methods in Molecular Biology series format, chapters include introductions to their respective topics, lists of the necessary materials and reagents, stepbystep, readily reproducible laboratory protocols, and tips on troubleshooting and avoiding known pitfalls. Authoritative and thorough, Nucleic Acid Crystallography Methods and Protocols presents protocols that are aimed at both researchers and students who are interested in the structural biology of DNA or RNA, alone or in complex with proteins or ligands.